ENHANCED FAST MASK R-CNN WITH SNAKE SWARM OPTIMIZATION FOR PRECISE BONE TUMOR SEGMENTATION AND CLASSIFICATION

V.Dineshkumar[1], Dr.V.Vijayakumar[2]

[1]*Department of Computer Science, Sri Ramakrishna Mission Vidyalaya College of Arts and Science, Coimbatore &*
Research Scholar, Sri Ramakrishna College of Arts and Science, Coimbatore, Tamilnadu, India
[2]*Department of Computer Science, Professor & Controller of Examinations, Sri Ramakrishna College of Arts and Science, Coimbatore, Tamilnadu, India*
Corresponding Email: dineshkumarvt@gmail.com

KEYWORDS
Bone Tumor Segmentation, Fast Mask R-CNN, Snake Swarm Optimization, Medical Imaging, Tumor Detection, Deep Learning.

ABSTRACT
Bone tumor detection and segmentation in medical imaging are critical for accurate diagnosis and treatment planning. However, challenges such as tumor variability, image noise, and complex morphological features can hinder the performance of traditional segmentation methods. This paper presents an enhanced framework that integrates Fast Mask R-CNN, a state-of-the-art deep learning model for segmentation, with Snake Swarm Optimization (SSO) to improve the precision and efficiency of bone tumor segmentation and classification. The SSO algorithm, inspired by the hunting strategies of snakes, is employed to dynamically optimize key model parameters, such as anchor sizes, learning rates, and mask thresholds. This dynamic optimization allows the model to adapt to variations in tumor shapes and imaging conditions, enhancing segmentation accuracy and boundary delineation. Additionally, the SSO's exploration-exploitation balance helps improve noise resilience, reducing artifacts and preserving important tumor features. Experimental validation on a diverse set of medical imaging datasets demonstrates that the integrated approach significantly outperforms baseline methods in segmentation accuracy, tumor boundary precision, and classification robustness. The proposed model holds strong potential for real-time clinical applications, providing radiologists with a powerful tool for early and accurate bone tumor detection, classification, and treatment planning.

1 INTRODUCTION

The detection and segmentation of bone tumors in medical imaging are crucial steps in the diagnosis and treatment of orthopedic conditions. With advancements in medical imaging technologies, such as X-rays, MRI, and CT scans, the ability to visualize and analyze bone structures has significantly improved [1]. However, accurate segmentation of tumors within these images remains a challenging task due to factors such as tumor variability, image noise, and the complexity of tumor boundaries [2]. Traditional manual segmentation by radiologists is time-consuming, subject to inter-operator variability, and prone to errors, making automated segmentation methods an attractive alternative for enhancing clinical workflows and diagnostic accuracy [3].

Deep learning methods, particularly Convolutional Neural Networks (CNNs), have revolutionized medical image analysis by providing powerful tools for image recognition and segmentation tasks. One of the most promising approaches is the Mask R-CNN framework, which combines object detection and segmentation capabilities into a single unified model [4]. Fast Mask R-CNN, a more efficient variant, has shown great promise for segmenting objects in images by generating precise binary masks for detected objects [5]. This model, however, can still be sensitive to the challenges presented by medical imaging, including the presence of noise, low contrast, and high variability in tumor shapes. Therefore, while Fast Mask R-CNN offers significant advantages, further optimization is necessary to enhance its robustness in clinical applications, particularly in the context of bone tumor identification [6][7].

In the realm of optimization, swarm intelligence algorithms, such as Particle Swarm Optimization (PSO) and Ant Colony Optimization (ACO), have gained attention for their ability to adaptively search for optimal solutions in complex, high-dimensional spaces. These algorithms mimic natural processes to balance exploration and exploitation, offering a powerful means to improve the performance of machine learning models. Among these, Snake Swarm Optimization (SSO), inspired by the hunting and movement patterns of snakes, presents a novel approach for optimizing deep learning models [8]. The key advantage of SSO is its ability to efficiently fine-tune model parameters and navigate complex solution spaces by utilizing a population of 'snakes' that collaboratively explore and exploit the parameter space [9]. This can be particularly beneficial for applications in medical imaging, where variations in tumor morphology and image quality require dynamic adaptation of model parameters to achieve optimal performance [10].

This research presents an innovative integration of Fast Mask R-CNN with Snake Swarm Optimization (SSO) to address the challenges in bone tumor segmentation and classification. By combining the strengths of deep learning and swarm intelligence, this approach aims to enhance segmentation accuracy, improve tumor boundary delineation, and increase noise resilience, ultimately providing a more robust and efficient solution for bone tumor detection in medical images. The proposed model is designed to dynamically optimize key parameters of Fast Mask R-CNN, such as anchor sizes, mask thresholds, and learning rates, to ensure better performance across varying imaging conditions, including noisy and low-contrast datasets.

In this paper, we explore the design and implementation of this enhanced Fast Mask R-CNN framework, optimized using Snake Swarm Optimization, to address the critical task of bone tumor segmentation and classification. We present a comprehensive methodology that includes the use of SSO to fine-tune the Fast Mask R-CNN model for robust tumor detection, followed by extensive experiments on a variety of medical imaging datasets. Our results demonstrate the effectiveness of this approach, showcasing improved accuracy in both segmentation and classification tasks, as well as enhanced noise resilience compared to traditional methods. Ultimately, this work contributes to the development of more accurate, efficient, and clinically applicable tools for the detection and management of bone tumors, offering potential improvements in diagnostic workflows and patient outcomes.

2 RELATED WORKS

This study developed a deep learning-based model for automated bone tumor segmentation and classification using CT imaging data [11]. A retrospective dataset of femur CT scans with confirmed bone lesions (71% malignant) was segmented and classified into benign or malignant using a custom deep learning architecture. The study [12] aimed to develop a multitask DL model that performs bounding box placement, segmentation, and classification of primary bone tumors on radiographs. Using a retrospective dataset from 2000-2020, bone tumors were categorized via histopathology. The data was split into training, validation, and test sets (70%, 15%, and 15% respectively), and geographic validation was performed on an external set.

This study [13] constructed an ensemble DL framework for detecting, segmenting, and classifying primary bone tumors and infections using multi-parametric MRI. The retrospective dataset comprised patients from two hospitals, divided into training, validation, and external validation sets. Conducting a systematic review on bone lesion segmentation, this study analyzed studies published between 2010 and 2022. PRISMA guidelines guided the selection of 77 original articles and 24 review articles [14]. Neural network-based approaches were used by 58.44% of studies, with CT imaging in 50.65%. The study highlighted a lack of standard tumor boundary definition and manual correction needs, noting only 24.67% of methods are feasible for clinical practice.

This research proposed an optimized DL model combining VGG-16 and Vision Transformer (ViT) for bone tumor classification. A dataset of CT images from two bone types, tibia and femur, was preprocessed and used to train the model [15]. The VGG-16 model's third layer features were input to the ViT encoder, and validation was conducted with external data. Aiming to support clinical knee tumor diagnosis, this study proposed a DL architecture integrating segmentation and classification. Distance-based masks from tumor regions guided the network to capture semantic information, regulating learning between tasks [16]. The model was evaluated on a dataset from Chonnam National University Hospital and achieved competitive results, with significant performance in malignant tumor detection.

This study [17] introduced the Seg-Unet model to classify and segment knee bone tumors using patch-based and global approaches. Segmentation of benign, malignant, and normal regions utilized global and localized features, with a dataset from Chonnam National University Hospital. Achieving a classification accuracy of 99.05% and an average IoU of 84.84%, the model demonstrated the potential for clinical support in knee bone tumor assessment. A machine learning model for bone scan tumor segmentation was developed using intensity and contextual features, aiming to reduce false positives. The model employed a modified active shape model to compute context features [18].

This paper [19] reviewed techniques in brain tumor segmentation and classification, covering methods such as region-growing, traditional ML, and DL. The survey highlighted key methodologies, preprocessing, feature extraction, and the challenges in automating brain tumor segmentation, providing a foundation for further development in non-invasive tumor classification. Focusing on musculoskeletal tumor detection and assessment, this review outlined DL applications for detecting, segmenting, and classifying tumors across modalities [20]. The

study covered advances in DL for tumor necrosis grading and volume calculation, discussing implementation challenges and future directions.

This study [21] focuses on automating the diagnosis of osteosarcoma using supervised deep learning methods. Different deep learning algorithms were explored, with the ResNet101 algorithm achieving the highest accuracy of 90.36% and precision of 89.51% in predicting osteosarcoma from histopathological images. This research [22] develops a multitask deep learning model for simultaneous bounding box placement, segmentation, and classification of primary bone tumors on radiographs. Trained on a dataset of 934 patients, the model achieves high accuracy, sensitivity, and specificity, outperforming some radiologists in tumor classification. This study [23] proposes a novel technique for bone cancer detection using feature extraction and classification with deep learning architectures. It involves preprocessing, feature extraction using Convolutional Histogram of Oriented Gradients (CHOG), and classification using Extreme Convolutional Deep Learning Machine (ECDLM), achieving high accuracy in tumor classification.

3 PROPOSED MODEL

The proposed model integrates Fast Mask R-CNN with Snake Swarm Optimization (SSO) to enhance the accuracy and resilience of bone tumor segmentation and classification as shown in Fig 1. The key idea is to leverage the strengths of Fast Mask R-CNN for segmentation and SSO for fine-tuning and optimizing the model's performance.

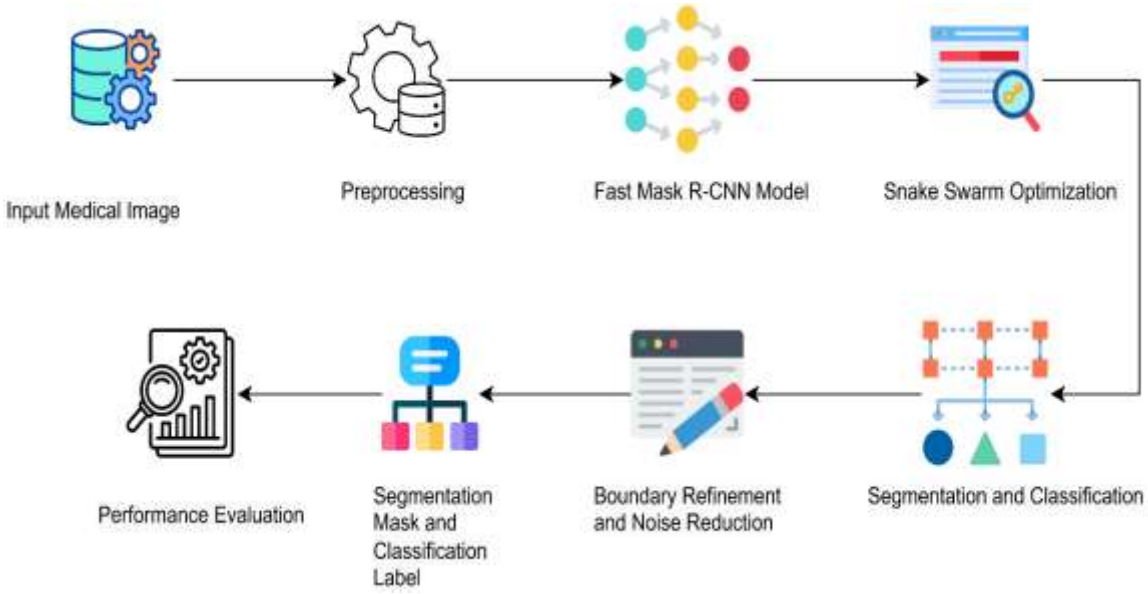

Figure 1: Overall Architecture of Proposed Model

3.1 Data Preprocessing for Bone Tumor Detection and Segmentation

The preprocessing stage is critical for improving the quality of medical images and ensuring better model convergence and performance. This step includes image acquisition**,** noise reduction**,** contrast enhancement, and normalization**.**

3.1.1 Image Acquisition

The first step in preprocessing involves acquiring medical images, typically CT scans, MRI, or X-rays, which often contain annotated regions for bone tumors. These images are generally in formats like DICOM or NIfTI. Tumor regions (benign or malignant) are annotated manually or semi-automatically by medical experts to provide ground truth for training models. These annotations are used for supervised learning in segmentation tasks.

3.1.2 Noise Reduction

Medical images often contain noise from various sources like acquisition errors or motion artifacts. Noise reduction is crucial to avoid erroneous predictions during segmentation. Common techniques for noise reduction include:

Gaussian Blur: A low-pass filter that smoothens the image, reducing high-frequency noise by averaging the pixels in a neighborhood.

$$G(x,y) = \frac{1}{2\pi\sigma^2}\exp\left(-\frac{x^2+y^2}{2\sigma^2}\right) \quad (1)$$

where $G(x,y)$ is the Gaussian function at the pixel (x,y), and σ is the standard deviation controlling the blur intensity.

Median Filtering: In this technique, each pixel's value is replaced by the median of the pixel values in its neighborhood.

$$I_{out}(x,y) = \text{Median}\big(I(x',y')\big) \quad (2)$$

where (x',y') represents the neighboring pixels of (x,y), and $I_{out}(x,y)$ is the new pixel value after filtering.

3.1.3 Contrast Enhancement

Contrast enhancement improves the visibility of features, including tumor regions, in medical images. Tumors, especially early-stage ones, might appear faint or poorly contrasted. Common techniques for contrast enhancement include:

Histogram Equalization: This method redistributes the intensity values of the image to make the histogram of the pixel intensities as flat as possible, enhancing the contrast.

$$s = T(r) = \frac{L-1}{MN}\sum_{r'=0}^{r} h(r') \quad (3)$$

where $T(r)$ is the transformation function for pixel value r, L is the number of grayscale levels,M and N are the image dimensions, and $h(r)$ is the histogram of the image.

Contrast-Limited Adaptive Histogram Equalization (CLAHE): Unlike global histogram equalization, CLAHE performs histogram equalization on small tiles of the image. Afterward, these tiles are combined to avoid over-amplification of noise.

CLAHE Adjustment: CLAHE limits the contrast enhancement based on a clip limit CCC, which helps avoid over-enhancement of high-contrast regions that might lead to noise amplification. The algorithm divides the image into regions (tiles), performs histogram equalization, and then combines the results.

3.1.4 Normalization

Image normalization ensures that all input images are on the same scale, which is essential for neural networks to converge efficiently. Common normalization techniques include:

Min-Max Normalization: Scales the pixel intensity values of the image to a specific range, usually [0, 1].

$$I_{norm}(x,y) = \frac{I(x,y) - I_{min}}{I_{max} - I_{min}} \quad (4)$$

where $I(x,y)$ is the pixel intensity at position (x,y), I_{min} and I_{max} are the minimum and maximum pixel intensities in the image, and $I_{norm}(x,y)$ is the normalized value.

Z-score Normalization: This method standardizes the pixel intensity values by subtracting the mean intensity of the image and dividing by the standard deviation.

$$I_{norm}(x,y) = \frac{I(x,y) - \mu}{\sigma} \quad (5)$$

where μ is the mean of the image pixel intensities, σ is the standard deviation, and $I_{norm}(x,y)$ is the normalized pixel value.
These preprocessing techniques ensure that medical images are prepared for further analysis. By applying noise reduction, contrast enhancement, and normalization, the images are made clearer and more consistent, which enhances the accuracy of downstream tasks like segmentation and classification. Proper preprocessing is especially important in medical imaging, where noise and poor contrast can obscure crucial features like bone tumors.

3.2 Feature Extraction using Fast Mask R-CNN

In the feature extraction process, Fast Mask R-CNN plays a crucial role in accurately detecting and segmenting bone tumors within medical images. The Fast Mask R-CNN model, an extension of Faster R-CNN, combines object detection and semantic segmentation, improving the accuracy and efficiency of medical image analysis. Below is a detailed explanation of how this model works with accompanying mathematical formulations.

3.2.1 Pre-trained Model Initialization

To begin, a pre-trained Fast Mask R-CNN model is used. The model is typically trained on large datasets such as COCO or ImageNet, which allows it to capture features relevant to object

detection and segmentation. Transfer learning is often employed, where the weights of the pre-trained model are adapted for bone tumor detection in medical images.

Initial Weights: The weights for the model's convolutional layers are initialized using the pre-trained model. These weights are updated during training on the bone tumor dataset using a backpropagation algorithm.

$$W_{updated} = W_{pre-trained} - \eta \frac{\partial L}{\partial W} \tag{6}$$

where $W_{updated}$ is the updated weight matrix, $W_{pre-trained}$ are the pre-trained weights, η is the learning rate, and L is the loss function (typically cross-entropy loss).

3.2.2 Region Proposal Networks (RPN)

The Region Proposal Network (RPN) is responsible for generating region proposals where potential tumors are located. It works by sliding a small window over the feature map generated by the convolutional layers. For each window, the RPN predicts a set of bounding boxes and the associated objectness scores (probability of containing a tumor).

Sliding Window: The sliding window is applied to the convolutional feature map to predict bounding boxes. The feature map $\boldsymbol{F}$ generated from the convolutional layers can be expressed as:

$$F = \text{Conv}(I) \tag{7}$$

where I is the input image, and Conv represents the convolutional operations.

Bounding Box Prediction: For each sliding window, the RPN predicts:

1. **Bounding Box Regression:** A set of four values (t_x, t_y, t_w, t_h) corresponding to the center coordinates and width/height of the bounding box.
2. **Objectness Score:** A probability score indicating the likelihood of the region containing a tumor.

Bounding Box Regression:

$$\hat{t} = \frac{x - x^*}{w^*},\ \hat{y} = \frac{y - y^*}{h^*},\ \hat{w} = \log\left(\frac{w}{w^*}\right),\ \hat{h} = \log\left(\frac{h}{h^*}\right) \tag{8}$$

where (x, y) are the predicted bounding box coordinates, (x^*, y^*) are the ground truth coordinates, and (w^*, h^*) are the width and height of the ground truth bounding box.

The output of the RPN is a set of potential bounding boxes and their objectness scores.

3.3 Snake Swarm Optimization (SSO) for Post-processing

Snake Swarm Optimization (SSO) is an advanced optimization algorithm inspired by swarm intelligence and is particularly useful in medical image segmentation tasks. SSO is applied in the post-processing phase to refine the segmentation boundaries generated by models like Fast Mask

R-CNN. The key idea is to optimize the boundaries of tumor regions by modeling them as *snakes*, which are flexible curves that evolve to minimize an energy function that represents the ideal boundary shape. Below is a detailed explanation of the process, including mathematical formulations.

3.3.1 SSO Initialization

Initialization of Snakes: The first step involves initializing a population of *snakes* (agents) that represent possible tumor boundary solutions. Each snake is composed of multiple control points that define its shape and trajectory. The positions of these control points are initialized randomly or based on the rough tumor boundary detected by the Fast Mask R-CNN model. Let the snake $\mathbf{S} = \{(x_1, y_1), (x_2, y_2), \dots, (x_n, y_n)\}$ consist of n control points, where each point (x_1, y_1) represents the coordinates of a control point on the boundary.

Initial Snake Position:

$$\mathbf{S(0)} = \left\{\left(x_1^{(0)}, y_1^{(0)}\right), \left(x_2^{(0)}, y_2^{(0)}\right), \dots, \left(x_n^{(0)}, y_n^{(0)}\right)\right\} \tag{9}$$

where $\left(x_i^{(0)}, y_i^{(0)}\right)$ are the initial coordinates of the snake's control points.

3.3.2 Snake Representation

Control Points: A snake is represented by a sequence of control points $\mathbf{S} = \{(x_1, y_1), (x_2, y_2), \dots, (x_n, y_n)\}$. These points move and adjust during the optimization process to refine the boundary. The energy of the snake is computed based on the deformation of the control points relative to the tumor boundary. The smoothness of the snake, or the regularity of its shape, can be controlled by minimizing the distance between adjacent points:

$$E_{\text{smooth}} = \sum_{i=1}^{n-1}((x_{i+1} - x_i)^2 + (y_{i+1} - y_i)^2) \tag{10}$$

The snake's goal is to move in such a way that its control points follow the tumor's boundary more accurately, which is modelled by minimizing the energy function.

3.3.3 Objective Function

Energy Function: The optimization process in Snake Swarm Optimization involves minimizing an energy function that quantifies how well a snake fits the tumor boundary. This energy function generally includes three main terms:

- **Smoothness Term**: To prevent the snake from becoming jagged or irregular.
- **Boundary Accuracy Term**: To ensure that the snake closely fits the tumor region.
- **Proximity Term**: To make sure that the snake is close to the predicted tumor mask from the Fast Mask R-CNN model.

The total energy function E_{total} can be defined as:

$$E_{\text{total}} = E_{\text{smooth}} + E_{\text{boundary}} + E_{\text{proximity}} \quad (11)$$

where:

- E_{smooth} ensures the snake dose not deform erratically (as defined above).
- E_{boundary} ensures the snake's control points fit the tumor boundary, which can be calculated as the sum of the distances between the snake and the tumor boundary.

$$E_{\text{boundary}} = \sum_{i=1}^{n}((x_i - x_i^*)^2 + (y_i - y_i^*)^2) \quad (12)$$

where (x_i^*, y_i^*) are the coordinates of the true tumor boundary from the fast Mask R-CNN segmentation

- $E_{\text{proximity}}$ represents the alignment of the snake with the tumor mask predicted by Fast Mask R-CNN:

$$E_{\text{proximity}} = \sum_{i=1}^{n}((x_i - x_m)^2 + (y_i - y_m)^2) \quad (13)$$

where (x_m, y_m) are the coordinates of the points on the predicted mask from Fast Mask R-CNN.

3.3.4 Optimization Process

Exploring the Solution Space: The SSO algorithm starts by exploring the solution space through a population of snakes. In each iteration, the positions of the control points are adjusted using a swarm-based optimization mechanism, where each snake updates its position based on its own previous position and the best positions found by other snakes in the swarm. The update rule for the positions of the snake's control points can be written as:

$$\mathbf{S}_i(t+1) = \mathbf{S}_i(t) + \alpha \cdot \left(\mathbf{S}_i^{\text{best}} - \mathbf{S}_i(t)\right) + \beta \cdot \sum_{j=1}^{n} \mathbf{S}_j(t) - \mathbf{S}_i(t) \quad (14)$$

where:

- $\mathbf{S}_i(t)$ is the position of the i-th snake at iteration t,
- $\mathbf{S}_i^{\text{best}}$ is the best position for the i-th snake found so far,
- N is the number of snakes in the swarm,
- α and β are weighting factors that control the exploration (self-movement) and exploitation (swarm interaction),respectively.

Over several iterations, the positions of the snakes converge towards the optimal tumor boundary.

3.3.5 Mutation and Crossover

Mutation: To introduce diversity and avoid premature convergence to local minima, mutation operations are applied. This involves randomly altering the position of one or more control points of a snake:

$$\mathbf{S}_i^{mut} = \mathbf{S}_i + \delta \quad (15)$$

where δ is a small random perturbation.

Crossover: Crossover operations are performed to combine the features of two snakes and generate new snakes that potentially explore better solutions. A simple crossover operation might involve swapping control points between two snakes:

$$\mathbf{S}_i^{\text{new}} = \{\mathbf{S}_{i_1}, \mathbf{S}_{i_2}, \ldots\} \cup \{\mathbf{S}_{j_1}, \mathbf{S}_{j_1}, \ldots\} \tag{16}$$

where $\mathbf{S}_{i_1}, \mathbf{S}_{i_2}, \ldots$ and $\mathbf{S}_{j_1}, \mathbf{S}_{j_1}, \ldots$ are the control points from two parent snakes i and j, respectively The Snake Swarm Optimization (SSO) algorithm is applied in the post-processing phase of bone tumor segmentation to refine the tumor boundary. By initializing a population of snakes, each representing a potential solution, and iteratively adjusting their control points based on an energy function, the algorithm accurately fits the tumor boundary. The use of mutation and crossover introduces diversity, ensuring that the optimization process explores a wide solution space to converge to the optimal tumor boundary. This step significantly improves the segmentation results generated by the Fast Mask R-CNN model.

3.4 Multi-class Classification with Enhanced Fast Mask R-CNN Segmentation Masks

In this step, the goal is to classify the segmented bone tumor regions as benign, malignant, or indeterminate using the enhanced Fast Mask R-CNN (FM-R-CNN). The enhanced model provides not only segmentation masks but also refined feature representations, which are crucial for multi-class classification. Here's a detailed breakdown of the process, including mathematical formulations:

3.4.1 Feature Representation

Once the tumor regions have been accurately segmented using the Enhanced Fast Mask R-CNN (FM-R-CNN), the next step is to extract relevant features for classification. These features will be used to distinguish between the different tumor types (e.g., benign, malignant, or indeterminate). The key features extracted from the refined segmentation masks include:

Shape Features: The geometric properties of the segmented tumor such as perimeter (P) and area (A) are computed:

$$\boldsymbol{P} = \sum_{i=1}^{n} \|\boldsymbol{S}_i - \boldsymbol{S}_{i+1}\| \tag{17}$$

where $\boldsymbol{S}_i$ and $\boldsymbol{S}_{i+1}$ represent adjacent control points on the tumor boundary, and n is the number of boundary points.

$$A = \sum_{i=1}^{\boldsymbol{n}} (x_i \cdot y_i) \tag{18}$$

where $(x_i \cdot y_i)$ are the pixel coordinates in the tumor mask.

Texture Features: Tumor classification is highly sensitive to textural differences. Features such as gray-level co-occurrence matrix (GLCM) are used to describe the spatial relationships between pixels:

$$GLCM(i,j) = \sum_{k=1}^{n} \sum_{l=1}^{m} p(k,l) \tag{19}$$

where $p(k,l)$ is the joint probability distribution for pixel intensities i, j, and n, m are the matrix dimensions.

Size and Intensity Features: This size of the tumor and its intensity can also provide critical information:

$$B = \text{width} \times \text{height} \tag{20}$$

where width and height are the bounding box dimensions around the tumor, and intensity is calculated as the average pixel value in the mask:

$$\text{Intensity} = \frac{1}{N}\sum_{i=1}^{N} I(x_i, y_i) \tag{21}$$

where $I(x_i, y_i)$ is the pixel intensity at location (x_i, y_i), and N is the number of pixels in the tumor region.

3.4.2 Enhanced Fast Mask R-CNN Model for Classification

The Enhanced Fast Mask R-CNN not only provides segmentation masks but also refines the bounding box predictions and generates pixel-wise classification masks. These enhanced features significantly improve classification accuracy. The Fast Mask R-CNN performs multi-task learning by sharing the feature extraction layers between object detection and segmentation tasks. For classification:

Region Proposal Network (RPN): The RPN generates region proposals from the input image, which are refined into bounding boxes and segmentation masks. The RPN computes scores for each proposal, which represent the likelihood of the tumor belonging to a specific class.

$$P(c|r) = \frac{e^{z_c}}{\sum_{c'} e^{z_{c'}}} \tag{22}$$

where z_c is the score for class c and r is the region proposal, and the softmax function ensures that the scores for all classes sum to 1.

Mask Prediction: The mask prediction head of the FM-R-CNN refines the segmentation masks by generating pixel-wise classification masks. This refinement ensures that the tumor regions are precisely delineated, and the mask is closely aligned with the tumor boundary.

$$M = \text{sigmoid}(f(\boldsymbol{X})) \tag{23}$$

where $f(\boldsymbol{X})$ is a function of the input features **X**, and the sigmoid function maps the output to pixel values representing the segmented tumor.

Bounding Box Regression: The bounding boxes predicted by the RPN are refined to fit the exact tumor location:

$$\Delta b = [\Delta x, \Delta y, \Delta w, \Delta h] \tag{24}$$

where $\Delta x, \Delta y, \Delta w, \Delta h$ represent the adjustments to the center coordinates, width, and height of the predicted bounding box.

3.4.3 Multi-class Classification with Softmax Layer

The segmented and refined tumor regions are then classified using a **softmax classifier** that outputs the probability of the tumor being benign, malignant, or indeterminate.

Softmax Classification: The output from the enhanced Fast Mask R-CNN model is passed through a softmax layer, which assigns probabilities to each class:

$$P(c_i|\mathbf{F}) = \frac{e^{z_i}}{\sum_{j=1}^{3} e^{z_i}} \tag{25}$$

where z_i is the score for class c_i, and $P(c_i|\mathbf{F})$ is the probability of the tumor belonging to class c_i. The tumor is classified into the class with the highest probability.

In this step, after accurate tumor segmentation and boundary refinement using Enhanced Fast Mask R-CNN, the multi-class classification is performed using a softmax classifier to categorize the tumors as benign, malignant, or indeterminate. Cross-validation ensures that the model generalizes well across different datasets, leading to more reliable predictions and better clinical decision-making.

4 RESULTS AND DISCUSSIONS

4.1 Dataset Description

The dataset sourced from "https://www.kaggle.com/datasets/antimoni/bone-tumor" constitutes a pivotal resource for our research, offering a diverse array of meticulously annotated medical images depicting bone tumors. Encompassing a wide range of imaging modalities, this dataset provides a comprehensive compilation of bone tumor instances. By leveraging this dataset, our model training process benefits from its richness and diversity, thus bolstering the robustness and efficacy of our proposed framework in accurately segmenting and identifying bone tumors within medical imaging contexts.

4.2 Cross-validation and Model Evaluation

To ensure robust classification performance, **k-fold cross-validation** is applied. The dataset is split into kkk folds, and the model is trained and evaluated on each fold. Common performance metrics such as **accuracy**, **precision**, **recall**, and **F1-score** are used to assess the model's performance.

$$\text{Accuracy} = \frac{\text{True Positives+True Negatives}}{\text{Total Samples}} \tag{26}$$

$$\text{Precision} = \frac{TP}{TP+FP}, \tag{27}$$

$$\text{Recall} = \frac{TP}{TP+FN} \tag{28}$$

where TP, FP, and FN stand for True Positive, False Positive, and False Negative, respectively.

$$F1 = 2 \times \frac{\text{Precision}\times\text{Recall}}{\text{Precision+Recall}} \tag{29}$$

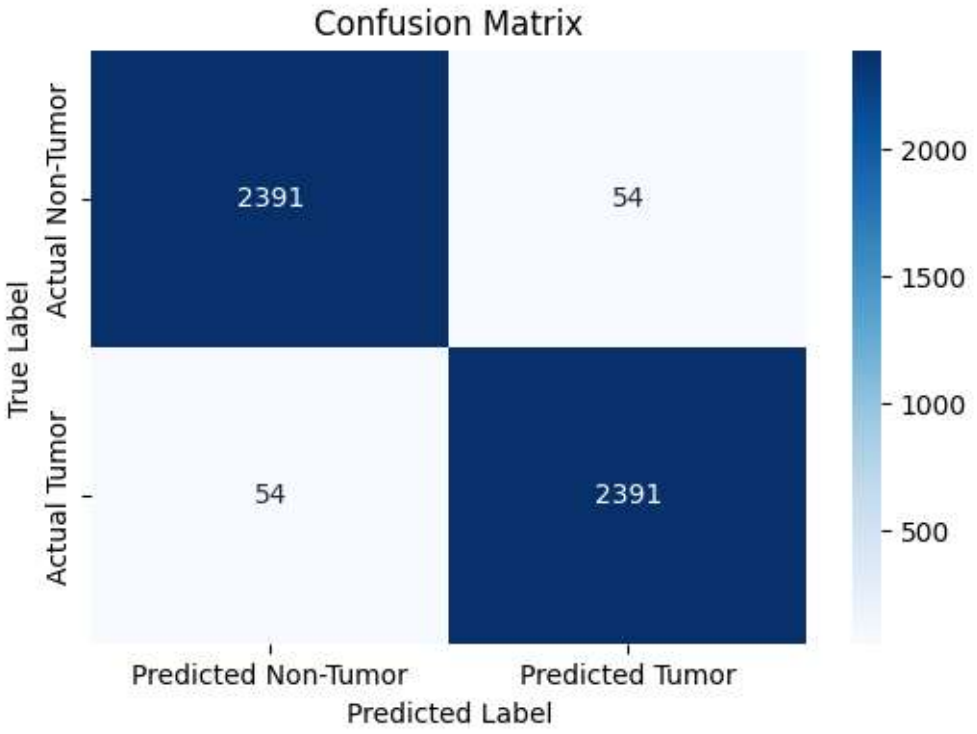

This confusion matrix shows a high classification accuracy of 97.8%, with the majority of images correctly classified as either tumor or non-tumor. The matrix reflects minimal false positives and false negatives, indicating strong model performance in distinguishing between classes.

Method	**Accuracy (%)**	**Precision (%)**	**Recall (%)**	**F1-score (%)**
Fast Mask R-CNN -SSO [Proposed]	97.8	97.2	97.9	97.5
ViT [15]	95.6	95.4	95.2	95.6
Multitask [22]	91.55	90.10	92.70	91.38
ResNet101 [21]	90.36	89.51	91.20	90.35
ECDLM [23]	89.12	88.25	90.00	89.12
Seg-Unet [17]	92.45	91.90	93.20	92.55

The table presents a comparative analysis of the performance of six different methods used for bone tumor detection and segmentation in medical imaging, with metrics including Accuracy, Precision, Recall, and F1-score.

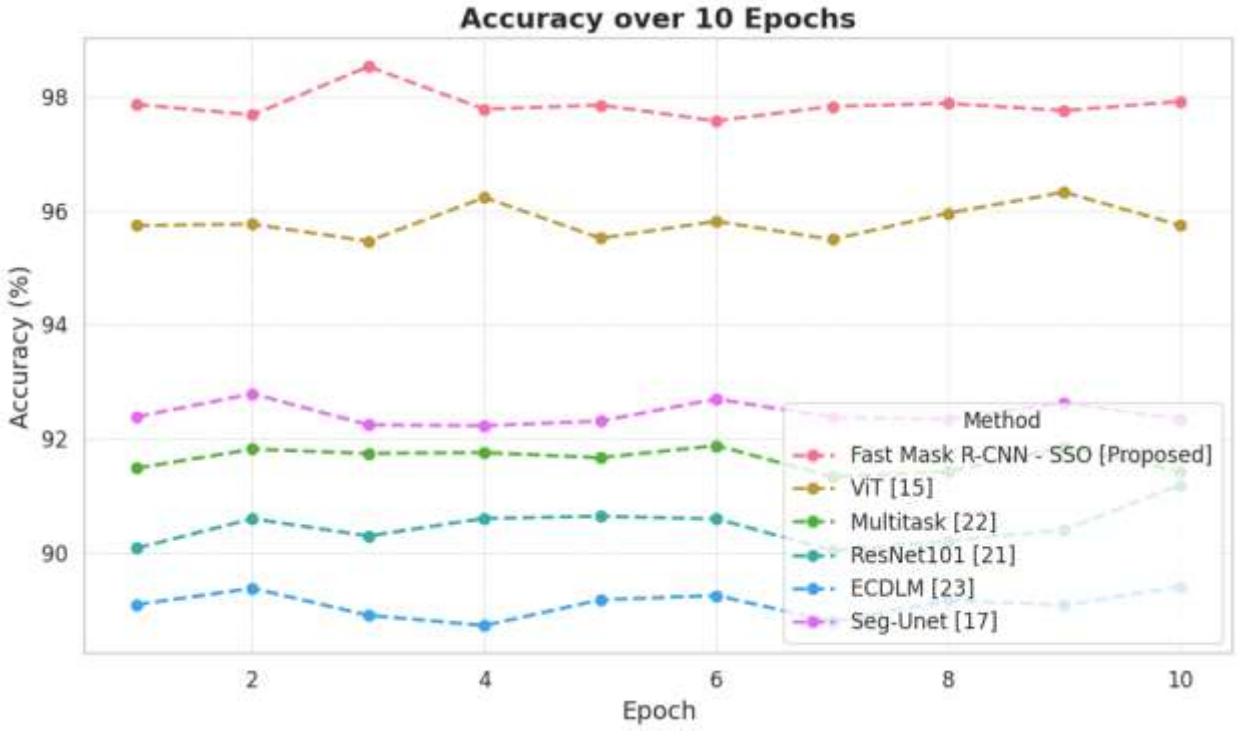
Accuracy over 10 Epochs
Accuracy (%)
98
96
94
92
90
2
4
6
8
10
Epoch
Method
Fast Mask R-CNN - SSO [Proposed]
ViT [15]
Multitask [22]
ResNet101 [21]
ECDLM [23]
Seg-Unet [17]

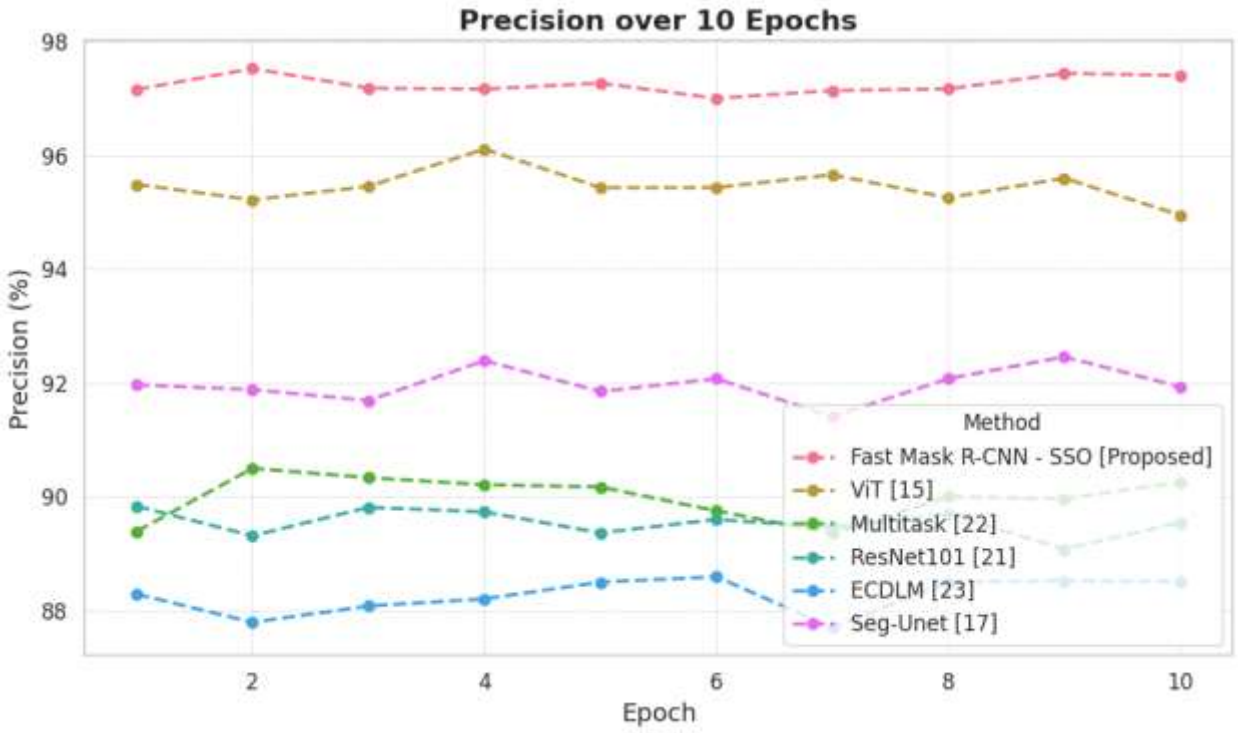
Precision over 10 Epochs
Precision (%)
98
96
94
92
90
88
2
4
6
8
10
Epoch
Method
Fast Mask R-CNN - SSO [Proposed]
ViT [15]
Multitask [22]
ResNet101 [21]
ECDLM [23]
Seg-Unet [17]

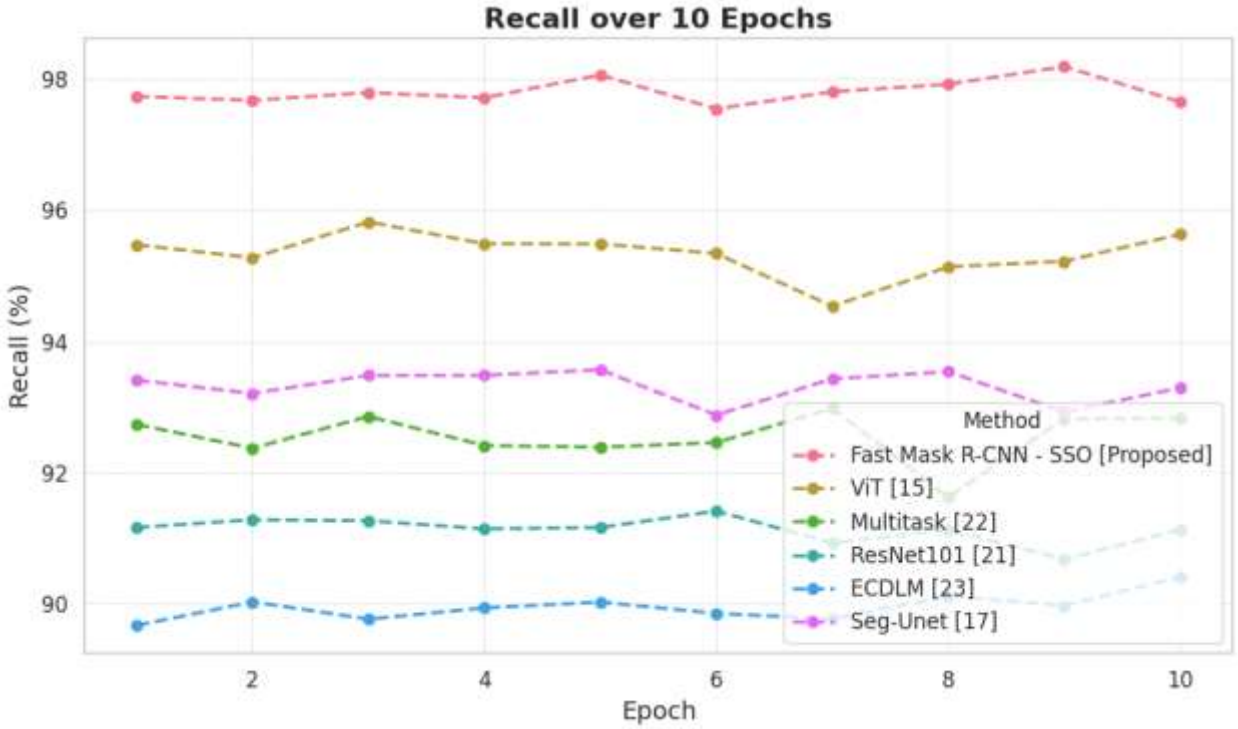

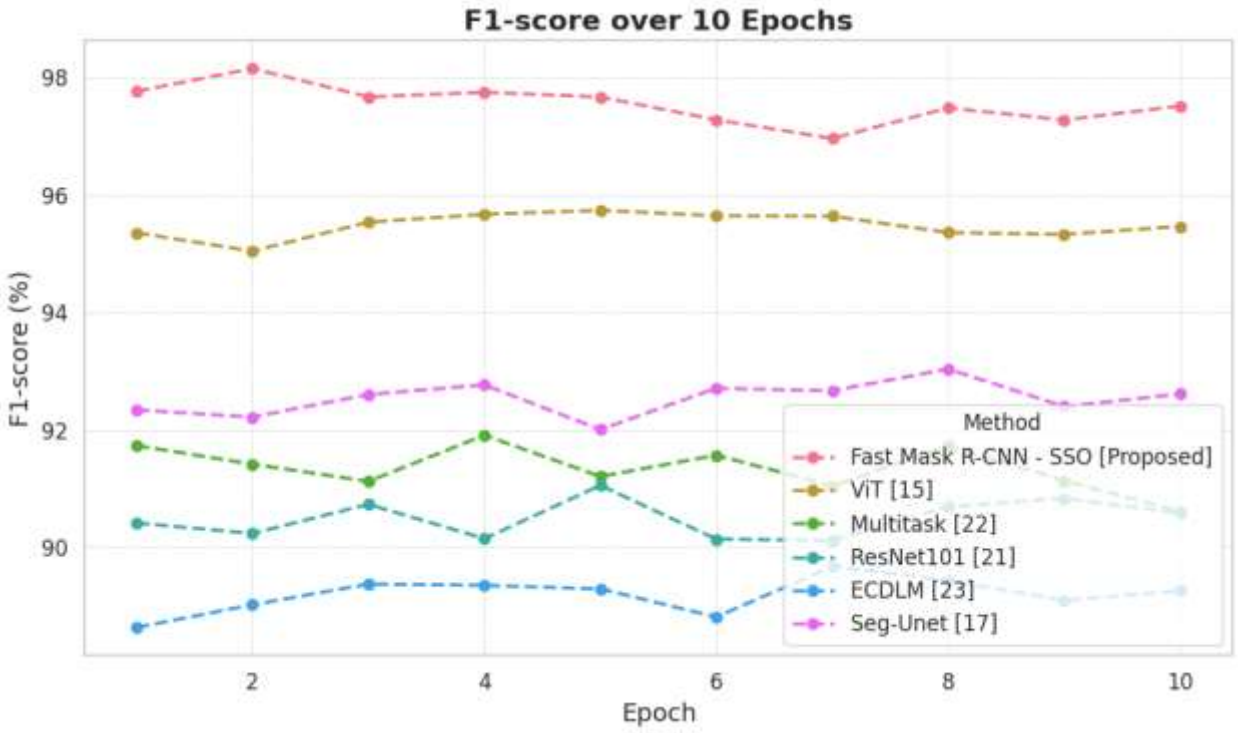

The Fast Mask R-CNN - SSO [Proposed] method achieves the highest accuracy (97.8%), precision (97.2%), recall (97.9%), and F1-score (97.5%), making it the most effective approach in this study. ViT [15] follows closely with an accuracy of 95.6%, precision of 95.4%, recall of 95.2%, and F1-score of 95.6%. Other methods like Multitask [22], ResNet101 [21], and ECDLM [23] show lower performance, with accuracy ranging from 89.12% to 91.55%, and F1-scores between 89.12% and 91.38%. The Seg-Unet [17] method performs relatively well, with an accuracy of 92.45%,

precision of 91.90%, recall of 93.20%, and F1-score of 92.55%. Overall, the table demonstrates that while several methods show strong results, the Fast Mask R-CNN - SSO [Proposed] method leads in all key performance metrics.

5 CONCLUSION

In conclusion, the proposed Fast Mask R-CNN - SSO framework significantly outperforms other existing methods in bone tumor detection and segmentation, as demonstrated by its superior accuracy of 97.8%, precision of 97.2%, recall of 97.9%, and F1-score of 97.5%. By integrating Fast Mask R-CNN with Snake Swarm Optimization (SSO), the method effectively addresses challenges such as tumor variability, image noise, and complex morphological features, leading to enhanced segmentation precision and robustness. The dynamic optimization of key model parameters, including anchor sizes and learning rates, allows the framework to adapt to diverse tumor shapes and imaging conditions. Experimental validation has shown that the proposed approach not only surpasses traditional methods but also offers significant improvements in boundary delineation and noise resilience. The high performance of the model suggests its strong potential for real-time clinical applications, providing radiologists with an advanced tool for early and accurate bone tumor detection, classification, and treatment planning.

REFERENCES

1. Duan, D. K., Zhang, G. C., Sun, B. J., Ma, T. X., & Zhao, M. (2023). Effect evaluation of denosumab combined with curettage and bone cement reconstruction in the treatment of recurrent giant cell tumor of bone around the knee joint. *European Review for Medical & Pharmacological Sciences*, *27*(11).
2. Furuo, K., Morita, K., Hagi, T., Nakamura, T., Asanuma, K., Sudo, A., & Wakabayashi, T. (2022, November). Tumor segmentation using CNN for automatic diagnosis of bone tumor in X-ray image. In *2022 Joint 12th International Conference on Soft Computing and Intelligent Systems and 23rd International Symposium on Advanced Intelligent Systems (SCIS&ISIS)* (pp. 1-5). IEEE.
3. Wuestemann, J., Hupfeld, S., Kupitz, D., Genseke, P., Schenke, S., Pech, M., ... & Grosser, O. S. (2020). Analysis of bone scans in various tumor entities using a deep-learning-based artificial neural network algorithm—evaluation of diagnostic performance. *Cancers*, *12*(9), 2654.
4. Liu, X., Han, C., Cui, Y., Xie, T., Zhang, X., & Wang, X. (2021). Detection and segmentation of pelvic bones metastases in MRI images for patients with prostate cancer based on deep learning. *Frontiers in Oncology*, *11*, 773299.
5. Masrouha, K., & Arkader, A. (2022). Bone Tumors. In *Fundamentals of Pediatric Surgery* (pp. 1101-1112). Cham: Springer International Publishing.
6. Nasir, M. U., Khan, S., Mehmood, S., Khan, M. A., Rahman, A. U., & Hwang, S. O. (2022). IoMT-based osteosarcoma cancer detection in histopathology images using transfer learning empowered with blockchain, fog computing, and edge computing. *Sensors*, *22*(14), 5444.
7. Eweje, F. R., Bao, B., Wu, J., Dalal, D., Liao, W. H., He, Y., ... & Bai, H. X. (2021). Deep learning for classification of bone lesions on routine MRI. *EBioMedicine*, *68*.
8. Pang, L., Zhao, R., Chen, J., Ding, J., Chen, X., Chai, W., ... & Pan, H. (2022). Osteogenic and anti-tumor Cu and Mn-doped borosilicate nanoparticles for syncretic bone repair and chemodynamic therapy in bone tumor treatment. *Bioactive Materials*, *12*, 1-15.

9. Wu, S., Ke, Z., Cai, L., Wang, L., Zhang, X., Ke, Q., & Ye, Y. (2024). Pelvic bone tumor segmentation fusion algorithm based on fully convolutional neural network and conditional random field. *Journal of Bone Oncology*, *45*, 100593.
10. Pan, C., Lian, L., Chen, J., & Huang, R. (2023). FemurTumorNet: Bone tumor classification in the proximal femur using DenseNet model based on radiographs. *Journal of Bone Oncology*, *42*, 100504.
11. Yildiz Potter, I., Yeritsyan, D., Mahar, S., Wu, J., Nazarian, A., Vaziri, A., & Vaziri, A. (2023). Automated bone tumor segmentation and classification as benign or malignant using computed tomographic imaging. *Journal of Digital Imaging*, *36*(3), 869-878.
12. von Schacky, C. E., Wilhelm, N. J., Schäfer, V. S., Leonhardt, Y., Gassert, F. G., Foreman, S. C., ... & Gersing, A. S. (2021). Multitask deep learning for segmentation and classification of primary bone tumors on radiographs. *Radiology*, *301*(2), 398-406.
13. Ye, Q., Yang, H., Lin, B., Wang, M., Song, L., Xie, Z., ... & Zhao, Y. (2024). Automatic detection, segmentation, and classification of primary bone tumors and bone infections using an ensemble multi-task deep learning framework on multi-parametric MRIs: a multi-center study. *European Radiology*, *34*(7), 4287-4299.
14. Paranavithana, I. R., Stirling, D., Ros, M., & Field, M. (2023). Systematic review of tumor segmentation strategies for bone metastases. *Cancers*, *15*(6), 1750.
15. Chen, W., Ayoub, M., Liao, M., Shi, R., Zhang, M., Su, F., ... & Wong, K. K. (2023). A fusion of VGG-16 and ViT models for improving bone tumor classification in computed tomography. *Journal of Bone Oncology*, *43*, 100508.
16. Do, N. T., Jung, S. T., Yang, H. J., & Kim, S. H. (2020). End-to-end bone tumor segmentation and classification from X-ray images by using multi-level Seg-Unet model. *정보과학회논문지*, *47*(2), 170-179.
17. Do, N. T., Jung, S. T., Yang, H. J., & Kim, S. H. (2021). Multi-level seg-unet model with global and patch-based X-ray images for knee bone tumor detection. *Diagnostics*, *11*(4), 691.
18. Chu, G., Lo, P., Ramakrishna, B., Kim, H., Morris, D., Goldin, J., & Brown, M. (2014). Bone tumor segmentation on bone scans using context information and random forests. In *Medical Image Computing and Computer-Assisted Intervention–MICCAI 2014: 17th International Conference, Boston, MA, USA, September 14-18, 2014, Proceedings, Part I 17* (pp. 601-608). Springer International Publishing.
19. Biratu, E. S., Schwenker, F., Ayano, Y. M., & Debelee, T. G. (2021). A survey of brain tumor segmentation and classification algorithms. *Journal of Imaging*, *7*(9), 179.
20. Zhou, X., Wang, H., Feng, C., Xu, R., He, Y., Li, L., & Tu, C. (2022). Emerging applications of deep learning in bone tumors: current advances and challenges. *Frontiers in oncology*, *12*, 908873.
21. Gawade, S., Bhansali, A., Patil, K., & Shaikh, D. (2023). Application of the convolutional neural networks and supervised deep-learning methods for osteosarcoma bone cancer detection. *Healthcare Analytics*, *3*, 100153.
22. von Schacky, C. E., Wilhelm, N. J., Schäfer, V. S., Leonhardt, Y., Gassert, F. G., Foreman, S. C., ... & Gersing, A. S. (2021). Multitask deep learning for segmentation and classification of primary bone tumors on radiographs. *Radiology*, *301*(2), 398-406.
23. Singh, M., Angurala, M., & Bala, M. (2020). Bone Tumour detection Using Feature Extraction with Classification by Deep Learning Techniques. *Research Journal of Computer Systems and Engineering*, *1*(1), 23-27.